# *L*-edge x-ray absorption in fcc and bcc Cu metal: Comparison of experimental and first-principles theoretical results

H. Ebert
*Institute for Physical Chemistry, University of Munich, Theresienstrasse 37, D-80333 München, Germany*

J. Stöhr, S. S. P. Parkin, and M. Samant
*IBM Research Division, Almaden Research Center, 650 Harry Road, San Jose, California 95120*

A. Nilsson
*Department of Physics, Uppsala University, Box 530, S-751 21 Uppsala, Sweden*
(Received 9 February 1996)

High resolution Cu $L_{2,3}$ x-ray absorption spectra of bulk fcc Cu metal are compared with those of thin Cu layers in Cu/Fe multilayers. Comparison of the measured fine structure with that obtained from a fully relativistic first-principles calculation for fcc and bcc Cu reveals that Cu is bcc in Cu(3 Å)/Fe(10 Å) and fcc in Cu(10 Å)/Fe(3 Å) multilayers. This result indicates that the thicker layer simply acts as a template for the structure of the thinner layer. The excellent agreement between experimental and theoretical spectra also demonstrates the validity of the theoretical approach. The theoretical spectra are discussed in terms of their angular momentum composition and the energy dependence of the radial transition matrix elements. [S0163-1829(96)03024-X]

## I. INTRODUCTION

Artificially layered structures where each layer consists of a different transition metal, a few atomic layers thick, exhibit a variety of scientific phenomena which are about to be utilized in technological devices. The discovery of giant magnetoresistance effects[1,2] and oscillatory exchange coupling,[3] for example, underlie the technology used in a spin-valve magnetic read head.[4,5] Similarly, layered structures with perpendicular magnetic anisotropy,[6,7] show promise as ''blue'' magneto-optical media.[8] It is expected that the magnetic properties of such multilayer structures may be strongly influenced by the crystal structures of the thin layers which are expected to differ from those of the bulk. The understanding of the correlation between magnetic and crystallographic structure in thin films is, therefore, an important problem.

A considerable amount of work has been carried out by the surface science community characterizing the magnetic and structural properties of thin layers grown on single crystal substrates. Relatively little work has been done on the structure of thin sandwiched and therefore buried layers, however, owing to the difficulty of most surface science techniques to probe below the surface. Another difficulty that is often encountered is the separation of the signals from the different layers in multilayerlike structures.

It is well established that the x-ray absorption fine structure (XAFS) above absorption edges is directly related to the local crystallographic structure around the absorbing atom.[9] Particular strengths of x-ray absorption spectroscopy are its element specificity and the fact that no long range crystallographic order of the sample is required. In the past, the most powerful use of XAFS for structural determinations has been the analysis of the fine structure above K absorption edges. Because *K*-edge absorption is governed by $s \rightarrow p$ dipole transitions, the analysis of the spectra is relatively simple.

Lately, *L*-edge XAFS studies of transition metals have become of great interest, since they allow access to the important *d* valence electrons through $p \rightarrow d$ dipole transitions. In particular, the investigation of absorption of circularly polarized x rays by magnetic materials, so called x-ray magnetic circular dichroism (XMCD) spectroscopy,[10] allows the direct determination of element-specific magnetic *d*-shell moments.[11–16] From a theoretical point of view, *L*-edge XAFS is complicated by the presence of $p \rightarrow s$ in addition to $p \rightarrow d$ transitions, and their relative contributions in the near edge region are not well understood. It is, therefore, highly desirable to obtain a better understanding of the information content of *L*-edge spectra in the region close to the absorption edge. It is the goal of the present paper to aid in this process.

Our studies report experimental data for the *L*-edge spectra of Cu metal, prepared in both fcc and bcc structures, by sandwiching a thin Cu layer between Fe layers of various thickness. The experimental spectra are compared to a fully relativistic first-principles calculation of the *L*-edge absorption spectra for fcc and bcc Cu metal. The sensitivity of the near edge structure to the crystallographical structure is convincingly demonstrated by comparison of experiment and theory. The theoretical results reveal quantitatively the various angular momentum contributions to the *L*-edge spectra.

## II. EXPERIMENTAL METHODS

The x-ray absorption spectrum of fcc Cu metal was recorded on a Cu(100) single crystal, which was cleaned *in situ* by ion sputtering and annealed to 600 °C prior to the measurement. All other samples were grown by dc magnetron sputtering as discussed before.[3] A 200 Å Cu film was grown

 

on Si(001), using a 100 Å Ru buffer layer and a 15 Å Ru capping layer to prevent oxidation. Its absorption spectrum was identical to that of the Cu single crystal. The Fe/Cu multilayer samples were grown as structures Fe(10 Å)/10[Cu(3 Å)/Fe(10 Å)] and Cu(10 Å)/10[Fe(3 Å)/Cu(10 Å)] onto a Si(100)/Ru(100 Å) substrate and covered with a Ru(15 Å) capping layer. These samples will be referred to as Cu(3)/Fe(10) and Cu(10)/Fe(3), respectively. In both samples the coupling between Fe layers is ferromagnetic and XMCD results on the Cu(3)/Fe(10) sample at both the Fe and Cu $L_{2,3}$ absorption edges have been reported previously.[17]

The high resolution x-ray absorption measurements were carried out at the Stanford Synchrotron Radiation Laboratory on the wiggler beam line 10–1, which is equipped with a spherical grating monochromator. We used 1000 l/mm holographic gratings and 10 $\mu$m entrance and exit slits, resulting in a resolution of about 0.3 eV at the Cu $L_3$ edge. Spectra were measured by recording the photocurrent of the sample with a picoammeter at normal x-ray incidence angle. The electron yield signal from a gold grid monitor was used to normalize the spectra to the incident photon flux.[18] After subtraction of a linear background fitted to the preedge region, the spectra were scaled to a unit step height far above the $L$ edges.

## III. CALCULATION OF THE ELECTRONIC STRUCTURE AND OF THE ABSORPTION SPECTRA

### A. Electronic structure

The electronic structure of fcc- and bcc-Cu has been calculated within the framework of the local density formalism, using the parametrization for the exchange-correlation potential due to Moruzzi *et al.*[19] For the fcc phase, the experimental lattice constant ($a_{\mathrm{fcc}}=6.83$ a.u.) has been used. That for the bcc phase has been chosen to give the same atomic volume ($a_{\mathrm{bcc}}=5.42$ a.u.). All work has been done using the Korringa-Kohn-Rostoker (KKR) method of band structure calculation in connection with the atomic sphere approximation.[20] This multiple scattering technique gives directly access to the electronic Green's function and, therefore, provides an extreme flexibility (see below). To account in a consistent way for all mechanisms that give rise to a difference in the x-ray absorption spectra at the $L_2$ and $L_3$ edges all calculations have been done in a fully relativistic way. The resulting density of states (DOS) curves for fcc-Cu resolved for the orbital angular momentum $\ell$ is shown in Fig. 1 for a wide range of energy. In addition the curves resolved according to the spin-orbit quantum number $\kappa$ are given, with $\kappa$ specifying the orbital angular momentum $\ell$ as well as the total angular momentum $j$ (e.g., $\kappa=-1,1,-2$, 2, and $-3$ corresponds to $s_{1/2}$, $p_{1/2}$, $p_{3/2}$, $d_{3/2}$, and $d_{5/2}$, respectively). As is well known, the electronic structure of fcc-Cu is characterized by a broad free-electron-like $sp$ band and a narrow $d$-band complex that lies about 1.4 eV below the Fermi energy. However, this crude description does not imply that the $d$-like states are completely filled. In fact, the number of $d$ electrons corresponding to the occupied part of the DOS curve is found to be 9.55. Furthermore, the $d$-like DOS around and above the Fermi energy is of the same order of magnitude as the other contributions. This also applies to the $f$ contributions, which is more or less negligible below the Fermi energy. Comparing the $\ell$-resolved DOS curves in Fig. 1 with results of corresponding nonrelativistic calculations (see, e.g., Ref. 19) no pronounced relativistic influences on the electronic structure are found. However, as can be seen in Fig. 1 for $\ell=2$, the $\kappa$-resolved DOS curves with $d_{3/2}$ and $d_{5/2}$ character differ remarkably in shape. This clearly manifests the importance of the spin-orbit coupling for the electronic structure of Cu, in spite of its relatively low

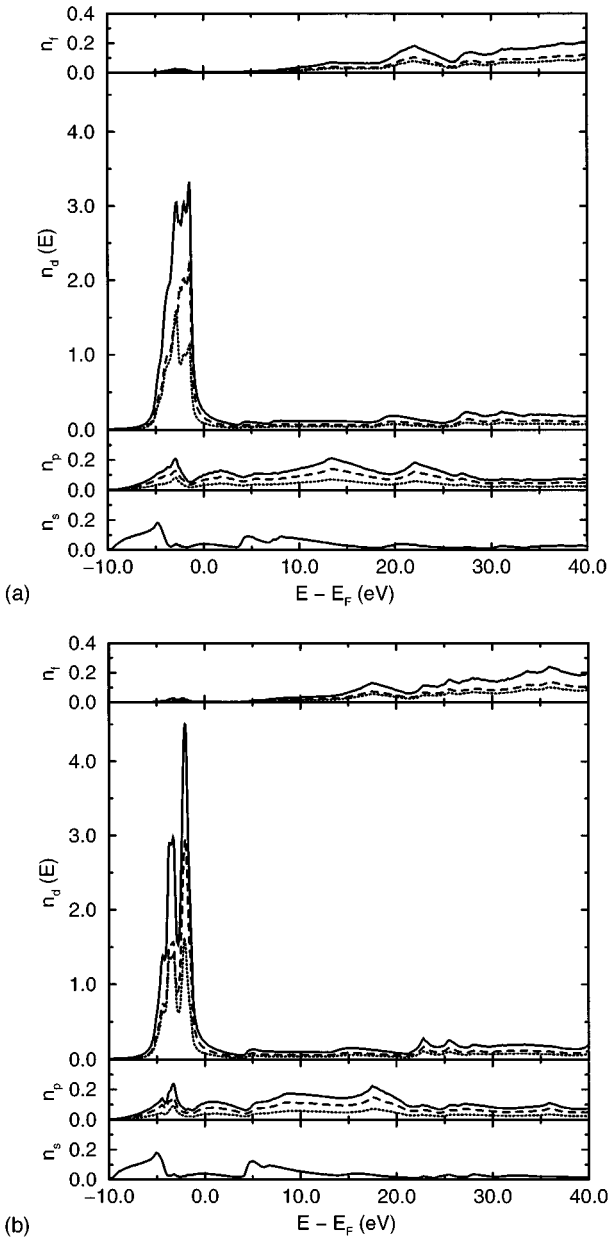


FIG. 1. Density of states curves $n_\ell(E)$ (full line) and $n_\kappa(E)$ (dotted line: $\kappa=+\ell$, i.e., $p_{1/2}$, $d_{3/2}$, and $f_{5/2}$; dashed line: $\kappa=-\ell-1$, i.e., $p_{3/2}$, $d_{5/2}$, and $f_{7/2}$), resolved according to the orbital angular momentum and spin-orbit quantum numbers $\ell$ and $\kappa$, respectively, for Cu in units of (states/atom eV). (a) and (b) give the results for the fcc and bcc structure, respectively. The density of states has been calculated for energies having a small imaginary part of 0.14 eV. The curves shown are, therefore, folded with a Lorentzian of the corresponding width.

atomic number. A further consequence of spin-orbit coupling for these DOS curves is that—in spite of their similar shape around the Fermi level—the ratio of the corresponding DOS values is below the ideal ratio 4:6. Because of the energy dependence of the spin-orbit coupling, the deviation from the ideal ratio gets rapidly smaller with increasing energy.

For bcc-Cu, the main features of the electronic structure are very similar to those of fcc-Cu. Of course, the detailed structure of the DOS curves differs, showing, for example, a clear separation of the *d* band into bonding and antibonding states as it is typical for metals with the bcc structure (see, e.g., Ref. 19).

### B. Calculation of the absorption spectra

Using Fermi's golden rule and adopting the electric dipole approximation, the x-ray absorption coefficient $\mu_\lambda(\omega)$ at the photon energy $\hbar\omega$ can be evaluated starting from the expression

$$\mu_\lambda(\hbar\omega)\propto \sum_{\substack{i\,\mathrm{occ}\\ n\mathbf{k}\,\mathrm{unocc}}} |\langle n\mathbf{k}|j_\lambda|i\rangle|^2\,\delta(E_{n\mathbf{k}}-E_i-\hbar\omega). \qquad (1)$$

Here, $|i\rangle$ and $|n\mathbf{k}\rangle$ represent the involved core and unoccupied band states, respectively. Within a fully relativistic calculation, the elements of the current density vector operator $j_\lambda$ are given by $-ec\alpha_\lambda$, with $\boldsymbol{\alpha}$ the vector of Dirac matrices and the index $\lambda$ specifying the polarization of the radiation. By making use of the identity

$$-\frac{1}{\pi}\mathrm{Im}G^+(E)=\sum_{n\mathbf{k}} |n\mathbf{k}\rangle\langle n\mathbf{k}|\,\delta(E_{n\mathbf{k}}-E), \qquad (2)$$

for the electronic Green's function $G^+(E)$, this expression can be transformed to the form[21]

$$\mu_\lambda(\hbar\omega)\propto\sum_{i\,\mathrm{occ}} \langle i|j_\lambda^\times \mathrm{Im}G^+(E_i+\hbar\omega)j_\lambda|i\rangle\,\theta(E_i+\hbar\omega-E_F), \qquad (3)$$

with $E_F$ the Fermi energy. This expression is the standard starting point for the extended x-ray absorption fine structure theory[21] and is also applicable for the x-ray absorption near edge structure region if the proper Green's function for the final states is used, i.e., the scattering for the electrons in the final state is not restricted to few neighboring atomic shells. Within the KKR formalism $\mathrm{Im}G^+$ is given by

$$\mathrm{Im}G^+(\mathbf{r},\mathbf{r}',E)=\sum_{\Lambda\Lambda'} Z_\Lambda(\mathbf{r},E)\mathrm{Im}\tau_{\Lambda\Lambda'}(E)Z^\times_{\Lambda'}(\mathbf{r}',E), \qquad (4)$$

with $\tau_{\Lambda\Lambda'}(E)$ the so-called scattering path operator and $Z_\Lambda(\mathbf{r},E)$ the regular solution to the Dirac equation normalized according to scattering theory.[22] The combined index $\Lambda$ represents the relativistic spin-orbit and magnetic quantum numbers, $\kappa$ and $\mu$, respectively.

Inserting Eq. (4) into Eq. (3) allows us to express $\mu_\lambda(\omega)$ in terms of the scattering path operator $\tau_{\Lambda\Lambda'}(E)$ and the matrix elements $\langle Z_\Lambda|ec\alpha_\lambda|\Phi_i\rangle$ with $\Phi_i(\mathbf{r},E_i)$ the core wave function. This approach is quite general and is even applicable for disordered systems. Furthermore, in its spin polarized relativistic form, it can be applied to magnetic systems and, therefore, gives access to the magnetic dichroism in x-ray absorption.[23] The expressions resulting from Eqs. (4) and (3) are given in detail in Ref. 23 and have been used here for the calculation of $\mu_\lambda(\omega)$.

For paramagnetic systems, the expression for $\mu_\lambda(\omega)$ can be further simplified. The first step is to replace the scattering path operator $\tau_{\Lambda\Lambda'}(E)$ with the $\kappa$-resolved density of states $n_\kappa(E)$ and accordingly the matrix elements $\langle Z_\Lambda|ec\alpha_\lambda|\Phi_i\rangle$ with $\langle \overline{Z_\Lambda}|ec\alpha_\lambda|\Phi_i\rangle$, where $\overline{Z_\Lambda}(\mathbf{r},E)$ is the wave function normalized to 1 within the atomic cell. Assuming unpolarized radiation the summation over the magnetic quantum number $\mu$ in Eq. (3) can be performed in a straightforward way, because the matrix elements can be split into an angular and radial part. As mentioned above, these matrix elements originally refer to the operator $-ec\alpha_\lambda$. This form has been used here to calculate $\mu_\lambda(\omega)$. Alternatively, one may replace $\langle \overline{Z_\Lambda}|ec\alpha_\lambda|\Phi_i\rangle$ by matrix elements with respect to the operators $\nabla$, $\nabla V$, or $\mathbf{r}$. The last form—the so-called configuration form—is numerically questionable,[24] but allows us to discuss the behavior of the resulting radial matrix elements in a straightforward way. Using that form, one finds for the $L_2$ and $L_3$ edges, the expressions[25–27]

$$\mu_{L_2}=\frac{1}{3}n_{s_{1/2}}R^2_{s_{1/2}p_{1/2}}+\frac{1}{3}n_{d_{3/2}}R^2_{d_{3/2}p_{1/2}}, \qquad (5)$$

$$\mu_{L_3}=\frac{2}{3}n_{s_{1/2}}R^2_{s_{1/2}p_{3/2}}+\frac{1}{15}n_{d_{3/2}}R^2_{d_{3/2}p_{3/2}}+\frac{2}{5}n_{d_{5/2}}R^2_{d_{5/2}p_{3/2}} \qquad (6)$$

which have been derived originally starting from Eq. (1) (Ref. 24) [the argument $E$ of $n_{\kappa_f}(E)$ and $R_{\kappa_f\kappa_i}(E)$ has been omitted]. Here, the $\kappa$-resolved density of states $n_\kappa(E)$ represents all contributions from the orbitals with character $\kappa$, i.e., it is not defined per orbital. The radial matrix elements occurring in Eqs. (5) and (6) are defined by

$$R_{\kappa_f\kappa_i}(E)=\int [g_{\kappa_f}(r,E)g_{\kappa_i}(r,E_i)+f_{\kappa_f}(r,E)f_{\kappa_i}(r,E_i)]r^3dr, \qquad (7)$$

with $g_{\kappa_f}(r,E)$ and $f_{\kappa_f}(r,E)$ the major and minor components of the wave function $\overline{Z_\Lambda}(\mathbf{r},E)$ for the final state and $g_{\kappa_i}(r,E_i)$ and $f_{\kappa_i}(r,E_i)$ for the initial state, respectively.

For a direct comparison with experiment, the spectra obtained from Eqs. (5) and (6) or Eqs. (3), respectively, still have to be broadened appropriately. To account for apparative broadening, a Gaussian function with a width of 0.4 eV has been used. All intrinsic broadening mechanisms as, e.g., the finite lifetime of the core hole were treated adopting the procedure suggested by Müller *et al.*,[28] using two Lorentzian functions with a constant and an energy dependent width, respectively. For the $L_2$ and $L_3$ edges the constant width parameter was set to 0.62 eV and 0.4 eV, respectively.[29]

## IV. RESULTS AND DISCUSSION

### A. Theoretical absorption spectrum

The theoretical absorption spectra are shown in Fig. 2. The lowest panel gives the decomposition of the spectra into $L_2$ and $L_3$ channels which are shifted against one another by

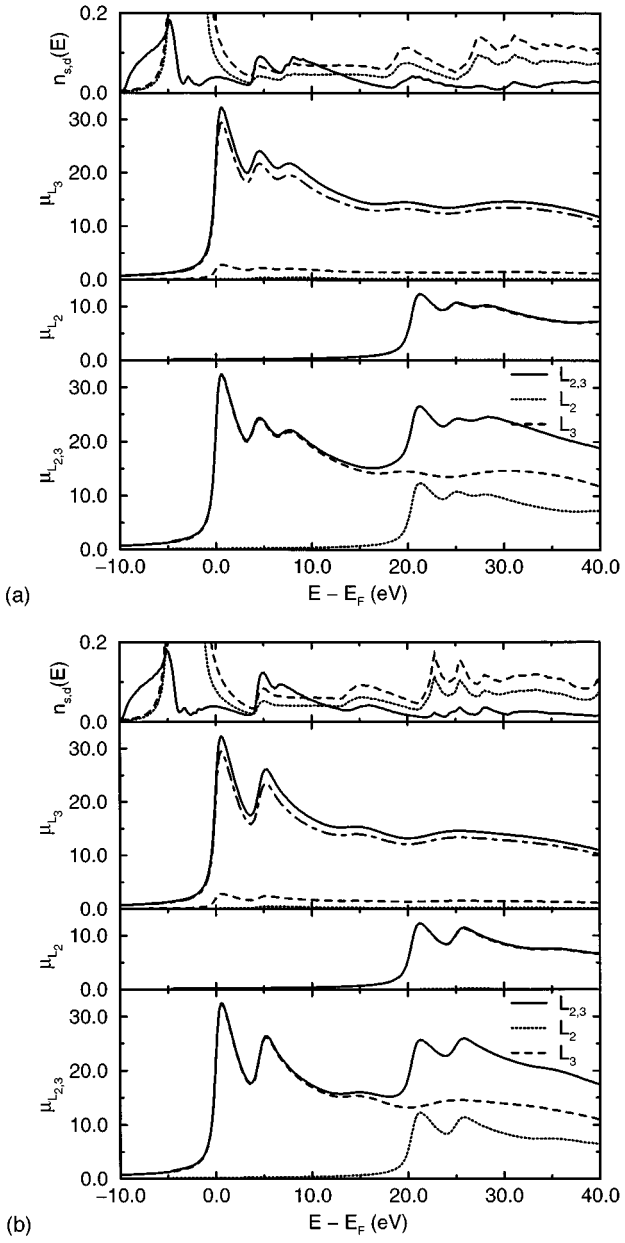


FIG. 2. Theoretical x-ray absorption coefficient $\mu_{L_{2,3}}$ for the $L_{2,3}$ edge of Cu. The lower panel gives the decomposition of $\mu_{L_{2,3}}$ according to the initial core states $2p_{1/2}$ and $2p_{3/2}$, i.e., into $L_2$- and $L_3$ spectra. These spectra are further decomposed according to the final states with $4s_{1/2}$, $3d_{3/2}$ and $3d_{5/2}$ character in the second and third panels. The uppermost panel gives the $s_{1/2}$, $d_{3/2}$, and $d_{5/2}$ resolved density of states as full, dotted, and dashed, respectively, lines from Fig. 1 for the sake of reference. (a) and (b) give the results for the fcc and bcc structure, respectively.

the spin-orbit splitting of the $2p$ states. This splitting was found to be 20.4 eV compared to 20.2 eV as deduced from core level x-ray photoemission spectroscopy.[30] The $L_2$ and $L_3$ spectra are very similar in shape with their relative magnitude close to 1:2, as expected from the numbers of states within the $2p_{1/2}$ and $2p_{3/2}$ subshells, respectively. Deviation from this ratio is to some extent due to the spin-orbit splitting within the $3d$ states, but also due to the stronger lifetime broadening for the $2p_{1/2}$ states compared to that of the $2p_{3/2}$ states.

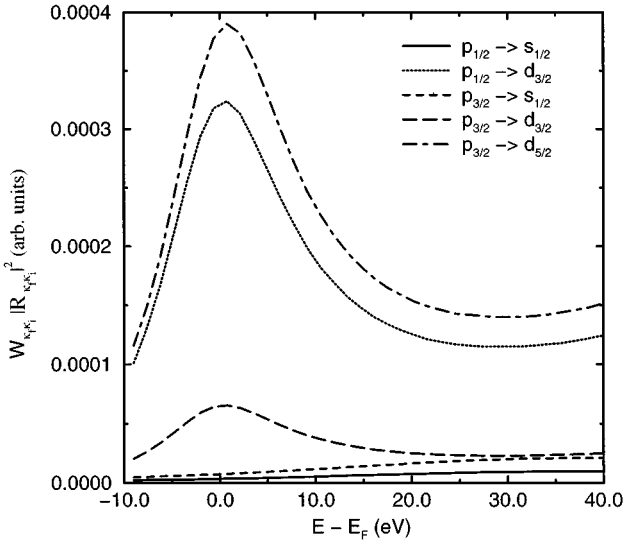


FIG. 3. Square of the radial x-ray absorption matrix elements $|R_{\kappa_f\kappa_i}(E)|^2$ of fcc-Cu according to Eq. (7) multiplied by the numerical prefactors $W_{\kappa_f\kappa_i}$ in Eqs. (5) and (6), as a function of the energy $E$ of the final state.

The DOS curves given in the top panel in Fig. 2 have been aligned to the $L_3$-absorption edge. Comparing the corresponding absorption spectrum with the DOS curve one finds—as expected from Eqs. (5) and (6)—that all structure in the spectrum can be traced back to corresponding peaks in the DOS curve. Inspection of the dispersion relation $E(\mathbf{k})$ in turn allows us to connect these peaks to regions in $\mathbf{k}$ space. For fcc-Cu, for example, the features at 4.5 and 7.5 eV stem from van Hove singularities at the $L$ and $X$ point in the Brillouin zone, where, due to the symmetry, $dE/dk$ vanishes leading to a band edge. For bcc-Cu, a singularity of the band structure at the $N$ point leads to a band edge giving rise to the feature at 5 eV in the DOS curves and the corresponding spectra.

Information on the relative importance of the $s$- and $d$-like partial DOS can be obtained by a decomposition of the $L_2$ and $L_3$ spectra, as it is given by the second and third panel in Fig. 2. For both spectra, one finds that the $s$-absorption channel contributes only 5% to the total absorption. This is partly due to the numerical prefactors in Eqs. (5) and (6) but predominantly, due to the radial matrix elements $R_{\kappa_f\kappa_i}(E)$, which are given in Fig. 3 as a function of energy. One of the main reasons that the $p$-$s$ matrix elements are so much smaller than the $p$-$d$ matrix elements seems to be the fact that the $2p$ and $3d$ radial wave functions, are nodeless functions, while the $4s$ wave function has three radial nodes. Furthermore—closely connected to this—the $3d$ wave function is stronger localized than the $4s$ wave function resulting in a stronger overlap with the $2p$ wave functions [see Eq. (7)].

The fact that the $s$-absorption channel plays only a minor role together with the weighting factors in Eq. (6) causes the $L_2$-edge spectrum to be dominated by the $d_{3/2}$-absorption channel (around 95%), while the $L_3$-edge spectrum is primarily due to the $d_{5/2}$-absorption channel (around 90%). The variation of the $d_{3/2}$- and $d_{5/2}$-DOS curves in the near edge

region mentioned above is, therefore, one of the main reasons that the peak at the $L_3$ edge is more pronounced than that at the $L_2$ edge.

As can be seen in Fig. 3, the matrix elements involving $3d$ states have a maximum close to the Fermi energy. For the energy range shown here, they decrease monotonously to about 40% of the maximum value at higher energies, until a flat minimum at 30 eV is reached. This property obviously emphasizes the absorption in the near-edge region and, therefore, enhances the white line. This behavior is further supported by the energy dependent Lorentzian linewidth (see above), which is meant to account for the energy dependent mean free path of the excited electron.[28] Within the energy range shown in Fig. 2, this mechanism increasingly washes out the structures in the absorption spectra for increasing energy. This is especially pronounced for the peaks at 27 and 31 eV in the case of the fcc structure and at 23 and 26 eV for the bcc structure, respectively. As a consequence of the energy dependent broadening, the $L_3$-absorption spectrum contribute for the range investigated here only slightly in the region of the $L_2$-absorption spectrum (see lowest panel of Fig. 2). This behavior is exemplified by the peak at 15 eV in the DOS curve of bcc-Cu. This is well below the $2p$ spin-orbit splitting and, therefore, the peak can be clearly seen in the total absorption spectrum. For the fcc structure, there is a corresponding peak at 20 eV. This is so close to the $L_2$ edge that the corresponding peak cannot be distinguished from the $L_2$-absorption spectrum. Nevertheless, the pronounced peaks in the DOS curves at higher energies (between 20 and 30 eV) result in a nonmonotonous background for the $L_2$-absorption spectrum. This is giving rise to an apparent change in the relative height of some peaks in the total spectrum as compared to the $L_3$-edge region. As one can see in the lower panel of Fig. 2 for the fcc structure the third peak at 29 eV in the $L_2$ region seems to be higher than the second one at 25 eV—in contrast to the $L_3$-edge region. For the bcc structure the second peak at 26 eV also seems to be higher than the first one at 21 eV—again in contrast to the $L_3$-edge region. That these relative heights read from the total spectrum are indeed spurious can clearly be seen from the $L_2$-absorption spectrum drawn separately in the lower panel of Fig. 2.

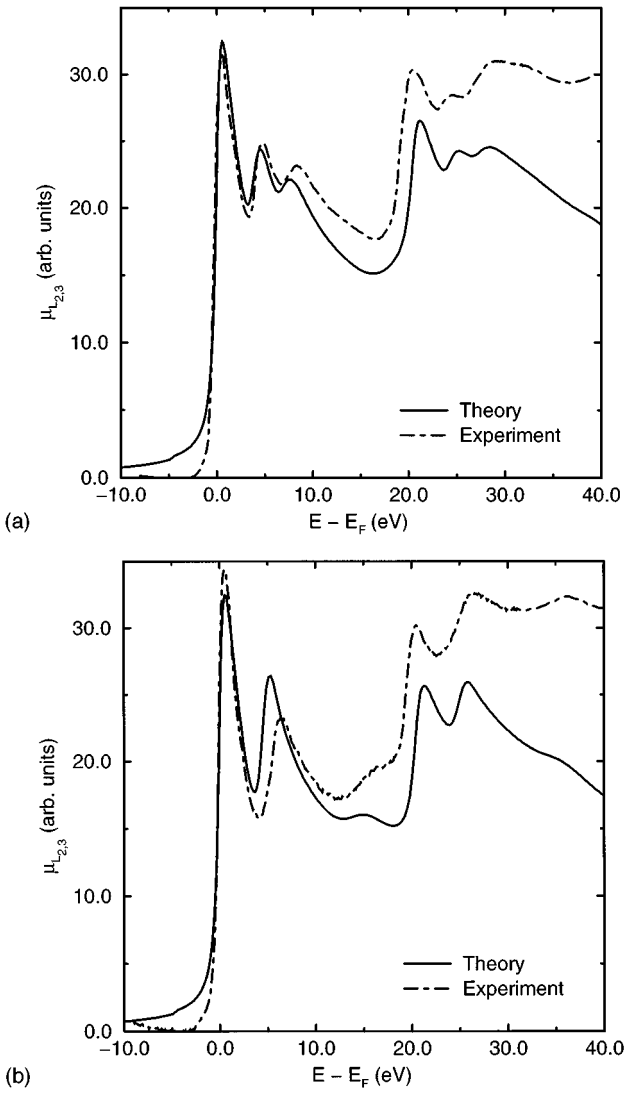


FIG. 4. Experimental and theoretical x-ray absorption coefficient $\mu_{L_{2,3}}$ for the $L_{2,3}$ edge of Cu. (a) and (b) give the results for the fcc and bcc structure, respectively. The experimental data for Cu with the bcc structure stems from the multilayer system Cu(3)/Fe(10) bcc.

### B. Comparison with experiment

The theoretical absorption spectra for fcc- and bcc-Cu discussed in the last section are compared in Fig. 4 with corresponding experimental data. As can be seen, a very satisfying agreement between experimental and theoretical data could be found for fcc-Cu, for which the proper structure was investigated experimentally. Deviations of both spectra from one another seem primarily caused by the background subtraction procedure for the experimental spectra. Because of this good agreement, the discussion and interpretation of the theoretical spectrum can be transferred directly to the experimental one. In summary, this means that the $L_2$ and $L_3$ spectra are nearly exclusively due to $2p_{1/2}-3d_{3/2}$ and $2p_{3/2}-3d_{5/2}$ transitions, respectively. This is a somewhat surprising feature because of the low lying $d$-band complex of Cu. Furthermore, the energy dependence of the radial matrix elements strongly enhances the white line at the absorption edge. All other prominent peaks in the spectrum can be traced back to band edges in the dispersion relation. Because of the overlap of the $L_3$ with the $L_2$ spectrum, the relative peak heights for the later can be read only with some uncertainty from the total spectrum. This feature, together with the spin-orbit splitting of the $d$ band, give rise to deviations of the $L_2$ to $L_3$ ratio at the absorption edges from the ideal one.

Figure 5 shows that the experimental $L_{2,3}$-absorption spectra of Cu in fcc-Cu and Cu(10)/Fe(3) are extremely similar. This means that for the multilayer system the Cu layers possess essentially fcc structure with a lattice constant close to that of pure fcc-Cu, in good accord with the observations of Pizzini *et al.*[32] The thin Fe interlayers adopt the imposed fcc-structure.[32] It might seem surprising that few—here ten—atomic layers are sufficient to show essentially the electronic structure of bulk Cu. However, this behavior is well known from angular resolved photoemission spectroscopy.

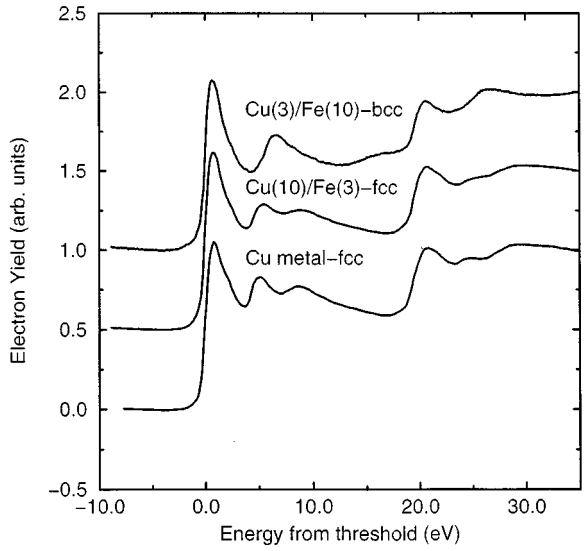


FIG. 5. Experimental x-ray absorption spectra at the $L_{2,3}$ edges of Cu. The various panels give from bottom to the top the spectra of Cu in pure fcc-Cu and in the multilayer systems Cu(10)/Fe(3) fcc and Cu(3)/Fe(10) bcc, respectively.

Here, few surface layers on a substrate are sufficient to give essentially the dispersion relation of the corresponding bulk material.[31]

In contrast to Cu(10)/Fe(3) for the Cu(3)/Fe(10) multilayer system, a Cu $L_{2,3}$-absorption spectrum is found that is very different from that of fcc-Cu (see Fig. 5). Obviously it is here that the thicker bcc-Fe layer imposes its structure on the thinner Cu-layers. This interpretation is strongly supported by the good agreement between the theoretical spectrum for bcc-Cu and the experimental one for the multilayer system. Assuming that the influence of the Fe adlayers on the electronic structure of Cu can be ignored, the agreement could presumably be further improved by choosing a more realistic lattice constant for bcc-Cu. Nevertheless, even without this optimization, the spectra in Fig. 4 convincingly demonstrate that for Cu(3)/Fe(10) it is the Fe subsystem that imposes its structure onto the total multilayer system. These results also support the observations of Pizzini *et al.*[32] Finally, it should be noted that—as for fcc-Cu—the good agreement of the theoretical and experimental spectra allows one to transfer the discussion and interpretation of the theoretical spectrum directly to the experimental one.

## V. SUMMARY

High resolution $L_{2,3}$ x-ray absorption spectra of Cu in bulk fcc-Cu, as well as Cu/Fe-multilayers have been presented together with corresponding first-principles calculations of these spectra. From a comparison of the various spectra, it could be concluded that, for the Cu(10)/Fe(3)-multilayer system, it is Cu that imposes the fcc structure onto the total system. For Cu(3)/Fe(10), on the other hand, it is the Fe that dictates altogether a bcc structure. All details of the experimental spectra could be explained and directly connected to the electronic structure with the help of the theoretical spectra. This demonstrates the usefulness of x-ray absorption spectroscopy as a probe for the local electronic structure, as well as the power of modern band structure calculations.

## ACKNOWLEDGMENT

This work was supported by the German ministry for research and technology (BMFT) under Contract No. 05 621WMA within the programme *Zirkular polarisierte Synchrotronstrahlung: Dichroismus, Magnetismus und Spinorientierung*.

[1] M. N. Baibich, J. M. Broto, A. Fert, F. N. V. Dau, F. Petroff, P. Eitenne, G. Creuzet, A. Friederich, and J. Chazelas, Phys. Rev. Lett. **61**, 2472 (1988).

[2] G. Binasch, P. Grünberg, F. Saurenbach, and W. Zinn, Phys. Rev. B **39**, 4828 (1989).

[3] S. S. P. Parkin, N. More, and K. P. Roche, Phys. Rev. Lett. **64**, 2304 (1990).

[4] B. Dieny, V. S. Speriosu, S. S. P. Parkin, B. A. Gurney, D. R. Wilhoit, and D. Mauri, Phys. Rev. B **43**, 1279 (1991).

[5] C. Tsang, R. E. Fontana Jr., T. Lin, D. E. Heim, V. S. Speriosu, B. A. Gurney, and M. L. Williams, IEEE Trans. Mag. **30**, 3801 (1994).

[6] U. Gradmann and J. Müller, Phys. Status Solidi **27**, 313 (1968).

[7] P. F. Carcia, A. D. Meinholdt, and A. Suna, Appl. Phys. Lett. **47**, 178 (1985).

[8] J. E. Hurst, Jr. and W. J. Kozlovsky, Jpn. J. Appl. Phys. **32**, 5301 (1993).

[9] *X-Ray Absorption: Principles, Applications, Techniques of EXAFS, SEXAFS and XANES*, edited by D. C. Koningsberger and R. Prins (Wiley, New York, 1988).

[10] G. Schütz, W. Wagner, W. Wilhelm, P. Kienle, R. Zeller, R. Frahm, and G. Materlik, Phys. Rev. Lett. **58**, 737 (1987).

[11] H. Ebert, B. Drittler, R. Zeller, and G. Schütz, Solid State Commun. **69**, 485 (1989); H. Ebert and R. Zeller, Phys. Rev. B **42**, 2744 (1990).

[12] C. T. Chen, F. Sette, Y. Ma, and S. Modesti, Phys. Rev. B **42**, 7262 (1990).

[13] G. van der Laan and B. T. Thole, Phys. Rev. B **43**, 13 401 (1991).

[14] F. Sette, C. T. Chen, Y. Ma, S. Modesti, and N. V. Smith, in *X-Ray Absorption Fine Structure*, edited by S. S. Hasnain (Ellis Horwood Limited, Chichester, England, 1991), p. 96.

[15] J. Stöhr, J. Electron Spectrosc. Relat. Phenom. **75**, 253 (1995).

[16] C. T. Chen, Y. U. Idzerda, H. J. Lin, N. V. Smith, G. Meigs, E. Chaban, G. H. Ho, E. Pellegrin, and F. Sette, Phys. Rev. Lett. **75**, 152 (1995).

[17] G. A. Held, M. G. Samant, J. Stöhr, S. S. P. Parkin, B. D. Hermsmeier, F. Herman, M. van Schilfgaarde, L. C. Duda, D. C. Mancini, N. Wassdahl, and R. Nakajima (unpublished).

[18] J. Stöhr, *NEXAFS Spectroscopy*, Springer Series in Surface Sciences Vol. 25 (Springer, Heidelberg, 1992).

[19] V. L. Moruzzi, J. F. Janak, and A. R. Williams, in *Calculated Electronic Properties of Metals* (Pergamon, New York, 1978).

[20] O. K. Andersen, Phys. Rev. B **12**, 3060 (1975).
[21] W. L. Schaich, Phys. Rev. B **42**, 6513 (1984).
[22] P. Strange, H. Ebert, J. B. Staunton, and B. L. Gyorffy, J. Phys. Condens. Matter **1**, 2959 (1989).
[23] H. Ebert and R. Zeller, Phys. Rev. B **42**, 2744 (1990).
[24] V. V. Nemoshkalenko, V. N. Antontonov, V. N. Antonov, and W. John, Phys. Status Solidi B **93**, 575 (1979).
[25] P. Weinberger and F. Rosicky, Theor. Chim. Acta. (Berlin) **48**, 349 (1978).
[26] L. F. Mattheiss and R. E. Dietz, Phys. Rev. B **22**, 1663 (1980).
[27] V. V. Nemoshkalenko *et al.*, Phys. Status Solidi B **111**, 11 (1982).
[28] J. E. Müller, O. Jepsen, and J. W. Wilkins, Solid State Commun. **42**, 365 (1982).
[29] J. C. Fuggle and J. E. Inglesfield, in *Unoccupied Electronic States*, edited by J. C. Fuggle and J. E. Inglesfield, Topics in Applied Physics, Vol. 69 (Springer, Berlin, 1992).
[30] L. Ley and M. Cardona, in *Photoemission in Solids II, Case Studies*, edited by L. Ley and M. Cardona, Topics in Applied Physics, Vol. 27 (Springer, Berlin, 1979).
[31] C. M. Schneider *et al.*, J. Phys. Condens. Matter **3**, 4349 (1991).
[32] S. Pizzini, F. Baudelet, D. Chandesris, A. Fontaine, H. Magnan, J. M. George, F. Petroff, A. Barthélemy, A. Fert, R. Loloee, and P. A. Schroeder, Phys. Rev. B **46**, 1253 (1992).